

High-efficient optical frequency mixing in all-dielectric metasurface empowered by multiple bound states in the continuum

TINGTING LIU^{1,6}, MEIBAO QIN², FENG WU³, AND SHUYUAN XIAO^{4,5,7}

¹*Institute of Photonic Chips, University of Shanghai for Science and Technology, Shanghai 200093, China*

²*School of Physics and Materials Science, Nanchang University, Nanchang 330031, China*

³*School of Optoelectronic Engineering, Guangdong Polytechnic Normal University, Guangzhou 510665, China*

⁴*Institute for Advanced Study, Nanchang University, Nanchang 330031, China*

⁵*Jiangxi Key Laboratory for Microscale Interdisciplinary Study, Nanchang University, Nanchang 330031, China*

⁶*e-mail: tliu@usst.edu.cn*

⁷*e-mail: syxiao@ncu.edu.cn*

Compiled September 20, 2022

We present nonlinear optical four-wave mixing in a silicon nanodisk dimer metasurface. Under the oblique incident plane waves, the designed metasurface exhibits a multi-resonant feature with simultaneous excitations of three quasi-bound states in the continuum (BIC). Through employing these quasi-BIC with maximizing electric field energy at the input bump wavelengths, significant enhancements of third-order nonlinear processes including third-harmonic generation, degenerate and non-degenerate four-wave mixing are demonstrated, giving rise to ten new frequencies in the visible wavelengths. This work may lead to a new frontier of ultracompact optical mixer for applications in optical circuitry, ultrasensitive sensing, and quantum nanophotonics. © 2022 Optica Publishing Group

<http://dx.doi.org/10.1364/ao.XX.XXXXXX>

Optical frequency mixing with efficient generation of new optical frequencies has found widespread use in various emerging research areas, including attosecond pulse generation, supercontinuum generation, optical frequency comb generation, material characterization, and quantum optics[1]. Amongst the nonlinear frequency conversion processes, four-wave mixing (FWM) is a versatile third-order nonlinear effect where four photons of different frequencies are mixed together with generated frequencies governed by the equation $\omega_{\text{FWM}} = \pm\omega_1 \pm \omega_2 \pm \omega_3$ in the case of three different incident photon frequencies ω_1 , ω_2 , and ω_3 . Recently, the ability to realize and harness FWM process at subwavelength volumes has become a popular pursuit in the community. A substantial progress in nonlinear frequency conversion at the nanoscale is achieved with the use of dielectric resonant metasurfaces[2, 3]. The high refractive index of dielectric material entails a large nonlinear susceptibility and the dielectric resonators confine electromagnetic fields inside. The dielectric metasurfaces underpin strong nonlinear response at the nanoscale as well as flexible control of nonlinear scattering,

when combined with the interplay between different multipolar resonances such as magnetic resonance[4–6], Fano resonance[7–9], and anapole excitation[10, 11].

A recently emerged concept of optical bound states in the continuum (BIC) has been developed to enhance optical frequency conversion in such systems. It provides an artificially intriguing approach to strongly confine and localize electromagnetic waves into subwavelength scale via multipolar control, which permits a direct link from ultrahigh quality (Q) factors excited in BIC dielectric metasurfaces to high-efficient nonlinear frequency conversion on chip. The electromagnetically engineered quasi-BIC supported by dielectric metasurfaces has been successfully utilized to enhance the second- (SHG)[12–14], third- (THG)[15, 16], and high-harmonic generation (HHG) processes[17, 18], up to a few orders of magnitude. Most recently, the BIC-assisted dielectric metasurface is demonstrated to generate efficiently high optical harmonics up to the 11th order[19]. Different from the harmonic generation processes above, FWM process is involved with different incident wavelengths and thereby the input wavelengths concurrently resonant is required for its efficiency enhancement[20–23]. However, up until now, enhanced FWM process empowered by the multiple BIC resonances of dielectric metasurfaces has rarely been explored.

In this work, we demonstrate high-efficient FWM processes in a dielectric metasurface by simultaneous excitations of multiple BIC resonances at input wavelengths. In the designed metasurface composed of silicon nanodisk dimers, the presences of the quasi-BIC resonances excited by γ -polarized oblique incident plane wave significantly increase the electric energy inside the structure. Together with the three-order nonlinear susceptibility of silicon, frequency mixing processes give rise to ten new frequencies spanning the visible region from ~ 450 nm to ~ 550 nm. The peak output power of these processes are achieved when the excitation wavelengths correspond to maximum of the internal electric energies at the quasi-BIC resonances.

Figure 1 shows a schematic of nonlinear optical frequency mixing processes in a silicon metasurface pumped by three laser beams. The metasurface consists of a periodic square array of

silicon nanodisk dimers, with a two-fold C_2 rotational symmetry. The lattice period is $p = 960$ nm. Each nanodisk has radius $r = 210$ nm and height $h = 280$ nm, and the distance between the two nanodisks is $d = 40$ nm. The refractive index of silicon are presented in Fig. S1 of Supplement 1.

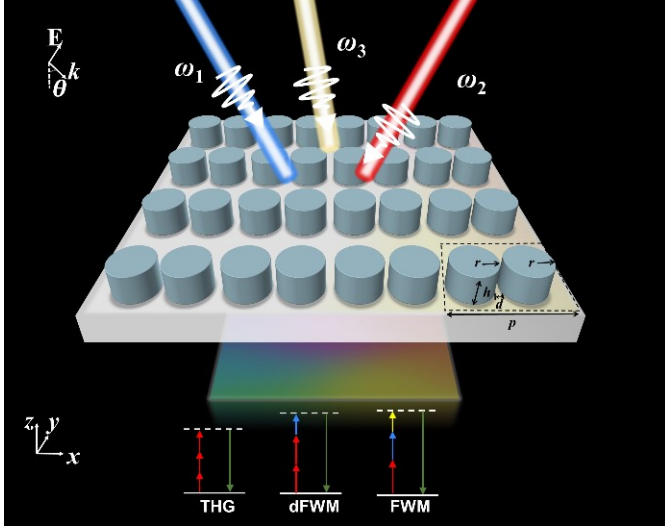


Fig. 1. The schematic of the designed metasurface consisting of a square array of silicon nanodisk dimers, simultaneously illuminated by three pump beams termed as ω_1 , ω_2 , and ω_3 in the near-infrared regime to generate a variety of new visible frequencies. The unit cell is indicated by a dotted square. The bottom inset illustrates the schematic energy diagrams of the nonlinear optical processes that occur simultaneously to generate visible emissions.

To boost the nonlinear optical frequency mixing, the designed metasurface simultaneously supports the BIC resonances at the wavelengths of the three input beams in the near-infrared regime. This can be confirmed by performing eigenmode analysis as well as by the simulated electromagnetic field profiles under y -polarized normal incidence in Fig. S2 of Supplement 1. Note that the distributions of the electromagnetic fields are even under C_2 around the z axis for eigenmodes 2, 3, and odd for mode 1, and thus these modes cannot be simultaneously excited by a normally incident plane wave whose electromagnetic fields are odd. As such, the y -polarized inclined plane waves are adopted to introduce the radiation leakage channels to transform the genuine BIC into the quasi-BIC resonances. Fig. 2(a) presents the evolutions of the transmission characteristics of the metasurface when the inclined incident angles are increased. The leaky resonances of quasi-BIC can be visualized with the observable finite linewidth of transmission under the oblique incidence. As a demonstration for resonantly enhanced frequency mixing, an incident angle of 10° is adopted here. In this case, the simulated transmission spectra of the metasurface exhibit the three narrow resonances around the corresponding wavelengths shown in Fig. 2(b). We estimate the Q factors of the quasi-BIC resonances by fitting the simulated transmission spectra with a Fano line shape expressed by $T = |a_1 + ia_2 + \frac{b}{\omega - \omega_0 + i\gamma}|^2$, where a_1 , a_2 , and b are real numbers, ω_0 is the resonance frequency of quasi-BIC, and γ is the total leakage rate [24, 25]. Meanwhile, the multipolar characteristics of each resonance is quantitatively identified using the Cartesian multipole decomposition, shown in Fig. S3 of Supplement 1. The asymmetric oblique incidence of light

triggers the transition from BIC to quasi-BIC resonances via small but perceptible interaction with the continuum, giving rise to the ultrahigh Q factors to increase the field enhancement.

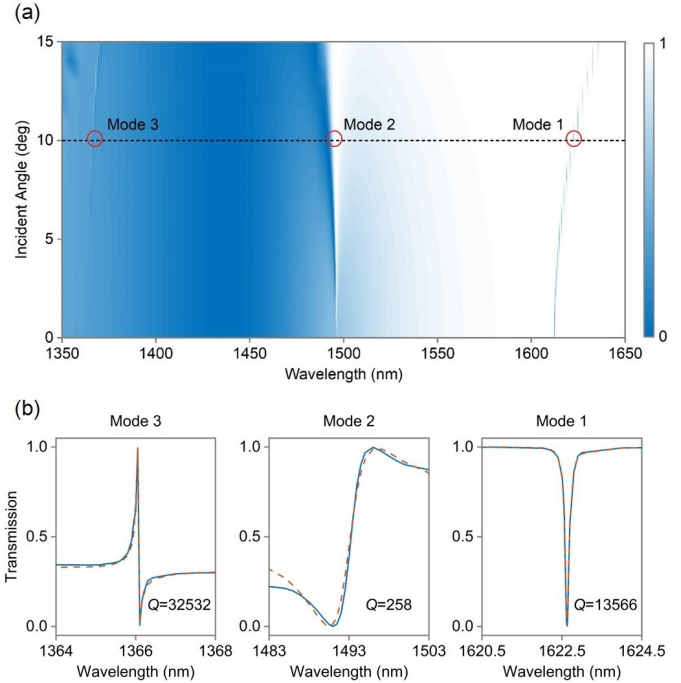


Fig. 2. (a) The transmission of the metasurface as a function of wavelength and incident angle. As seen, the resonances corresponding to the excitations of the three quasi-BIC modes show narrow linewidth, when the modes evolve from the perfect BIC to quasi-BIC. (b) The simulated (solid) and theoretical (dashed) transmission spectra of the metasurface under y -polarized oblique incidence of 10° in the vicinity of the three quasi-BIC resonances.

The nonlinear response is simulated with the frequency domain solver in COMSOL MULTIPHYSICS through two sequential computations. The electric field at the fundamental wavelength are computed in the first step and then a nonlinear polarization density is induced as the source term of the wave equation in the second step. For the silicon material considered here, the nonlinear polarization associated with the third-order nonlinear process can be expressed by [1]

$$P_i(\omega_1 + \omega_2 + \omega_3) = \varepsilon_0 D \sum_{ijkl} \chi_{ijkl}^{(3)} E_j(\omega_1) E_k(\omega_2) E_l(\omega_3), \quad (1)$$

where ε_0 is the vacuum permittivity, D is the degeneracy factor, $\chi^{(3)}$ is the third-order nonlinear susceptibility of silicon, and E is the localized electric field at the fundamental wavelength. Here $\chi^{(3)} = 2.45 \times 10^{-19} \text{ m}^2/\text{V}^2$ is adopted for silicon in the near-infrared, and the optical intensity of fundamental pump is fixed to $1 \text{ MW}/\text{cm}^2$.

To start with, we study the harmonic generations by the metasurface when pumped by a single near-infrared beam. In Fig. 3, the envelope of the THG power spectrum presents three distinctive peaks at 455.35 nm, 497.67 nm, and 540.88 nm, respectively. Since the third-order nonlinear effect essentially behaves as a volume phenomenon, we use the volume electric energy at the excitation wavelengths to characterize the excitation power here. As shown in Fig. 3, the electric energy stored in the resonators

reaches the peak values at the quasi-BIC resonance wavelengths corresponding to the modes 1, 2, 3 as anticipated, in consistent with the BIC feature to effectively confining the electric field inside the dielectric resonators. The essential connection between the nonlinear emission and internal electric field energy explains the very good agreement between the three peaks of THG power and the three maxima of electric energy. Intriguingly, although resonance mode 1 shows lower Q -factor and field enhancement at fundamental wavelength 1622.63 nm than those of mode 3 at 1366.05 nm, the peak of THG power corresponding to mode 1 at the wavelength 540.88 nm is approximately 5 times larger than the peak power of mode 3 at 455.35 nm because of the relatively larger electric energy. Their efficiency difference originates from the fact that the electric field of quasi-BIC resonance at mode 1 is preferentially located inside the nanodisks, rather than that near the edges at mode 3, which is a more beneficial aspect for nonlinear THG processes with large volume contribution.

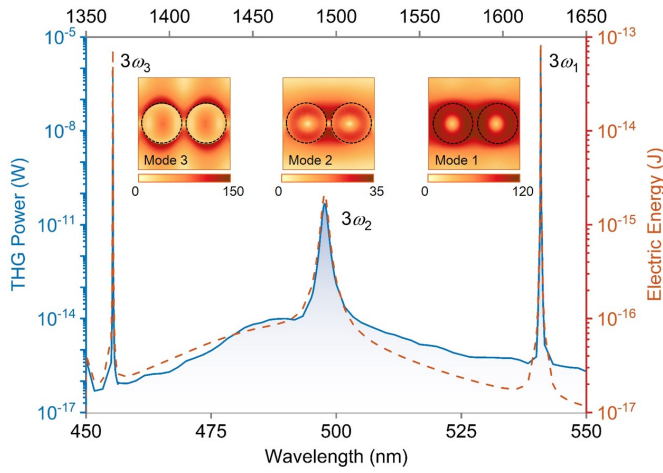


Fig. 3. The THG power (solid) and electric energy inside the nanodisk dimers (dashed) of the metasurface under y -polarized oblique incidence. Insets are the enhancement of electric field intensity ($|E|/|E_0|$) at the fundamental wavelengths of the three quasi-BIC resonances.

Due to the presence of multiple quasi-BIC resonances in the designed metasurface, it is possible to study FWM by exciting either single or multiple modes. Justified by the enhanced THG signals in Fig. 3, the combination of highly confined electromagnetic fields within the nanodisk dimers and the strong intrinsic material nonlinearities of silicon should allow FWM process to be effectively exploited. Fig. 4 shows the results of mixing different excitation frequencies at the three quasi-BIC resonances at ω_1 , ω_2 , and ω_3 , respectively. When the three pump beams are temporally coincident, the ten spectral peaks ranging from ~ 450 nm to ~ 550 nm can be obtained in the visible window. In Figs. 4(a)-(c), two pump beams are considered with one at a fixed wavelength of ω_1 , ω_2 , and ω_3 , respectively, and in Fig. 4(d), another pump beam is introduced with two fixed wavelengths at ω_1 and ω_2 . For easy comparisons, the optical intensity of input pumps are all fixed at $1 \text{ MW}/\text{cm}^2$ in the simulations.

The generated optical mixing signals can be categorized into three groups. The first group corresponds to the THG processes when the input beams have the same frequencies. Note the THG powers here are about 2 orders of magnitude larger than those in Fig. 3, because the input power comes from the two input pumps here. The second group consists of the degener-

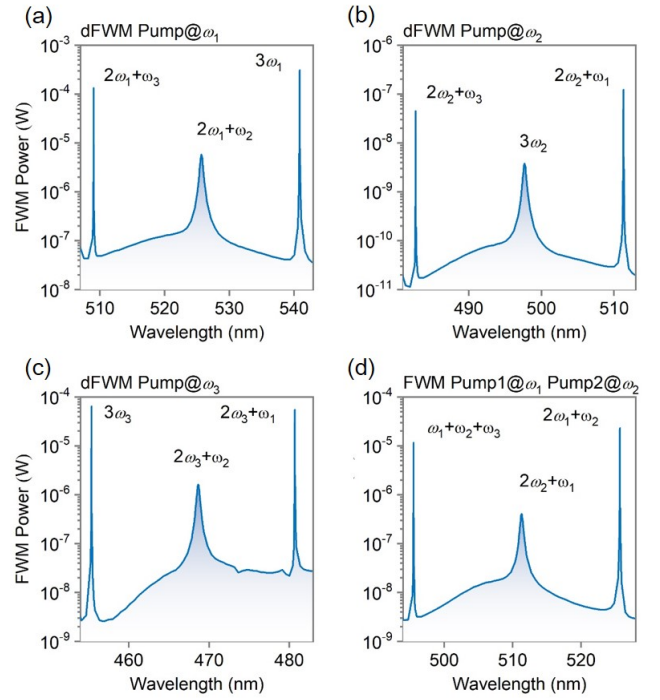


Fig. 4. The nonlinearly generated visible signals originating from optical frequency mixing under y -polarized oblique incidence when the multiple beams simultaneously pump the metasurface. (a)-(c) Two pump beams are considered with one at a fixed wavelength of ω_1 , ω_2 , and ω_3 , respectively. (d) Three pump beams are considered with two fixed wavelengths at ω_1 and ω_2 .

ate four-wave mixing (dFWM) processes, $2\omega_1 + \omega_3$, $2\omega_1 + \omega_2$, $2\omega_2 + \omega_3$, $2\omega_2 + \omega_1$, $2\omega_3 + \omega_2$, $2\omega_3 + \omega_1$, with peaks at 509 nm, 525.66 nm, 482.71 nm, 511.28 nm, 468.63 nm, 480.69 nm, respectively. The powers of these dFWM peaks do not simply scale as the product of Q factors of the involved quasi-BIC modes. Instead, similarly with THG powers dependent on the internal electric energy, the dFWM radiations are determined by the combination of highly confined fields and spatial overlap of the quasi-BIC modes involved, for example in Fig. 4(b), the dFWM signals at $2\omega_2 + \omega_1$ is ~ 2.7 times larger than that at $2\omega_2 + \omega_3$. The third group corresponds to the non-dFWM process with a new frequency of $\omega_1 + \omega_2 + \omega_3$ when the three different bumps simultaneously illuminate on the metasurface. Thanks to the simultaneous occurrence of the three quasi-BIC resonances at the input wavelengths, the FWM peak reaches $1.17 \times 10^{-5} \text{ W}$, and it is the first time to obtain such an enhanced non-dFWM in metasurface systems.

Finally, we study the power dependence of these third-order nonlinear processes. Fig. 5 shows a log-log plot of the output powers with respect to incident excitation power upon the metasurface. Here the THG process, dFWM, and non-dFWM processes at new frequencies of $3\omega_1$, $2\omega_1 + \omega_2$, and $\omega_1 + \omega_2 + \omega_3$ and different pump powers at ω_1 are taken as typical examples from the three categories. As can be seen, the power of the non-dFWM process increases linearly with the excitation power at ω_1 when the other pump power is held constant. Meanwhile, a quadratic dependence of dFWM process $2\omega_1 + \omega_2$ on the ω_1 pump power can be also observed, and this rule would also be suitable for other degenerate processes. For the THG pro-

cesses, a slope value of 3 is observed as expected, implying a cube dependence of the output power on the excitation power. These power dependences verify the typical characteristics of third-order nonlinear effects[20–23].

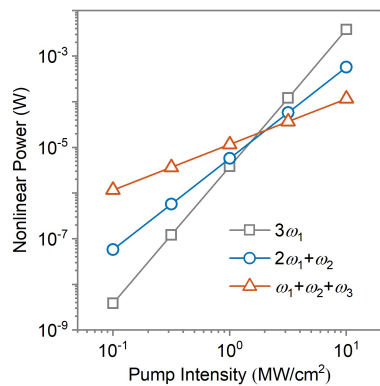


Fig. 5. The power dependence of nonlinear third-order frequency mixing processes including THG ($3\omega_1$), dFWM ($2\omega_1 + \omega_2$), and non-dFWM ($\omega_1 + \omega_2 + \omega_3$) on the power of the ω_1 pump.

In summary, we have demonstrated high-efficient FWM processes in multiple-BIC resonant metasurface composed of silicon nanodisk dimers. Under the oblique incidence, three quasi-BIC resonances with ultrahigh Q-factors are simultaneously excited in the near-infrared wavelengths, leading to the enhanced electric field and thus the large internal electric energy beneficial for boosting nonlinear effects. Taking advantage of the multiple quasi-BIC resonances at the input wavelengths, the third-order frequency mixing processes in silicon metasurface obtain dramatic enhancement, and ten new frequencies in visible wavelengths can be observed arising from THG, dFWM and non-dFWM processes. Our work expands substantially the range of applications of BIC dielectric metasurfaces in highly efficient nonlinear metadevices, and will stimulate advances in miniaturized frequency mixing systems. Finally, it is worth pointing out that the design and mechanism in this work are general, and can be applied to other nonlinear optical effects, in particular, the photon pair generation via spontaneous parametric down-conversion[26, 27].

Funding. National Natural Science Foundation of China (11947065, 61901164, 12104105, 12264028); Natural Science Foundation of Jiangxi Province (20202BAB211007); Interdisciplinary Innovation Fund of Nanchang University (2019-9166-27060003); Open Project of Shandong Provincial Key Laboratory of Optics and Photonic Devices (K202102); Start-up Funding of Guangdong Polytechnic Normal University (2021SDKYA033); China Scholarship Council (202008420045).

Disclosures. The authors declare no conflicts of interest.

Data Availability Statement. Data underlying the results presented in this paper are not publicly available at this time but may be obtained from the authors upon reasonable request.

Supplemental document. See Supplement 1 for supporting content.

REFERENCES

- R. W. Boyd, *Nonlinear Optics* (Academic Press, New York, 2020).
- B. Sain, C. Meier, and T. Zentgraf, *Adv. Photonics* **1**, 024002 (2019).
- T. Liu, S. Xiao, B. Li, M. Gu, H. Luan, and X. Fang, *Front. Nanotechnol.* **4**, 891892 (2022).
- L. Carletti, A. Locatelli, O. Stepanenko, G. Leo, and C. D. Angelis, *Opt. Express* **23**, 26544 (2015).
- Y. Gao, Y. Fan, Y. Wang, W. Yang, Q. Song, and S. Xiao, *Nano Lett.* **18**, 8054 (2018).
- T. Liu, X. Fang, and S. Xiao, *Phys. Rev. B* **104**, 195428 (2021).
- Y. Yang, W. Wang, A. Boulesbaa, I. I. Kravchenko, D. P. Briggs, A. Poretzky, D. Geohegan, and J. Valentine, *Nano Lett.* **15**, 7388 (2015).
- P. P. Vabishchevich, S. Liu, M. B. Sinclair, G. A. Keeler, G. M. Peake, and I. Brener, *ACS Photonics* **5**, 1685 (2018).
- G. Ban, C. Gong, C. Zhou, S. Li, R. Barille, X. Liu, and Y. Wang, *Opt. Lett.* **44**, 126 (2018).
- G. Grinblat, Y. Li, M. P. Nielsen, R. F. Oulton, and S. A. Maier, *Nano Lett.* **16**, 4635 (2016).
- L. Xu, M. Rahmani, K. Z. Kamali, A. Lamprianidis, L. Ghirardini, J. Sautter, R. Camacho-Morales, H. Chen, M. Parry, I. Staude, G. Zhang, D. Neshev, and A. E. Miroshnichenko, *Light Sci. Appl.* **7**, 44 (2018).
- A. P. Anthur, H. Zhang, R. Paniagua-Dominguez, D. A. Kalashnikov, S. T. Ha, T. W. W. Maß, A. I. Kuznetsov, and L. Krivitsky, *Nano Lett.* **20**, 8745 (2020).
- T. Ning, X. Li, Z. Zhang, Y. Huo, Q. Yue, L. Zhao, and Y. Gao, *Opt. Express* **29**, 17286 (2021).
- Z. Huang, M. Wang, Y. Li, J. Shang, K. Li, W. Qiu, J. Dong, H. Guan, Z. Chen, and H. Lu, *Nanotechnology* **32**, 325207 (2021).
- L. Xu, K. Z. Kamali, L. Huang, M. Rahmani, A. Smirnov, R. Camacho-Morales, Y. Ma, G. Zhang, M. Woolley, D. Neshev, and A. E. Miroshnichenko, *Adv. Sci.* **6**, 1802119 (2019).
- Z. Liu, Y. Xu, Y. Lin, J. Xiang, T. Feng, Q. Cao, J. Li, S. Lan, and J. Liu, *Phys. Rev. Lett.* **123**, 253901 (2019).
- L. Carletti, S. S. Kruk, A. A. Bogdanov, C. D. Angelis, and Y. Kivshar, *Phys. Rev. Res.* **1**, 023016 (2019).
- S. Xiao, M. Qin, J. Duan, F. Wu, and T. Liu, *Phys. Rev. B* **105**, 195440 (2022).
- G. Zograf, K. Koshelev, A. Zalogina, V. Korolev, R. Hollinger, D.-Y. Choi, M. Zuerch, C. Spielmann, B. Luther-Davies, D. Kartashov, S. V. Makarov, S. S. Kruk, and Y. Kivshar, *ACS Photonics* **9**, 567 (2022).
- G. Grinblat, Y. Li, M. P. Nielsen, R. F. Oulton, and S. A. Maier, *ACS Photonics* **4**, 2144 (2017).
- S. Liu, P. P. Vabishchevich, A. Vaskin, J. L. Reno, G. A. Keeler, M. B. Sinclair, I. Staude, and I. Brener, *Nat. Commun.* **9**, 2507 (2018).
- R. Colom, L. Xu, L. Marini, F. Bedu, I. Ozerov, T. Begou, J. Lumeau, A. E. Miroshnichenko, D. Neshev, B. T. Kuhlmeier, S. Palomba, and N. Bonod, *ACS Photonics* **6**, 1295 (2019).
- L. Xu, D. A. Smirnova, R. Camacho-Morales, R. A. Aoni, K. Z. Kamali, M. Cai, C. Ying, Z. Zheng, A. E. Miroshnichenko, D. N. Neshev, and M. Rahmani, *New J. Phys.* **24**, 035002 (2022).
- Y. He, G. Guo, T. Feng, Y. Xu, and A. E. Miroshnichenko, *Phys. Rev. B* **98**, 161112 (2018).
- M. Qin, J. Duan, S. Xiao, W. Liu, T. Yu, T. Wang, and Q. Liao, *Phys. Rev. B* **105**, 195425 (2022).
- T. Santiago-Cruz, S. D. Gennaro, O. Mitrofanov, S. Addamane, J. Reno, I. Brener, and M. V. Chekhova, *Science* **377**, 991 (2022).
- J. Zhang, J. Ma, M. Parry, M. Cai, R. Camacho-Morales, L. Xu, D. N. Neshev, and A. A. Sukhorukov, *Sci. Adv.* **8**, eabq4240 (2022).